Journal of the Korean Physical Society, Vol. 75, No. 1, July 2019, pp. 45∼53

Fiber Positioner Based on Flexible Hinges Amplification Mechanism

Xue CHENG
Changchun Institute of Optics, Fine Mechanics and Physics, Chinese Academy of Sciences, Changchun 130033, China and University of Chinese Academy of Sciences, Beijing 100049, China

Jian-Li WANG
Changchun Institute of Optics, Fine Mechanics and Physics, Chinese Academy of Sciences, Changchun 130033, China

Chang-Hua LIU
Changchun Institute of Optics, Fine Mechanics and Physics, Chinese Academy of Sciences, Changchun 130033, China and University of Chinese Academy of Sciences, Beijing 100049, China

Liang WANG* and Xu-dong LIN
Changchun Institute of Optics, Fine Mechanics and Physics, Chinese Academy of Sciences, Changchun 130033, China

(Received 10 April 2019; revised 20 May 2019; accepted 21 May 2019)

Due to the nonlinear effect and the thermal effect, a single optical fiber has limitations in the output power. A beam combination of laser arrays based on adaptive optics can both improve the output power and ensure higher beam quality. This article puts forward one novel fiber positioner structure based on the flexible hinges amplification mechanism, which is the adaptive fiber optics collimator (AFOC), to correct tip-tilt aberration. The theoretical model was established, and the amplification ratios between the output displacement and device's structure parameters were calculated. The first 6 orders of the mode shape of the vibration of amplification mechanism was obtained by using a modal analysis. Analysis results revealed an excellent performance for the flexible hinges amplification mechanism. The novel fiber positioner has good prospects for applications in laser beam combination systems for ideal tip-tilt control.

PACS numbers: 42.81.Wg, 95.75.Qr, 07.60.Vg, 42.62.−b
Keywords: Fiber positioner, Adaptive optics, Flexible hinges amplification mechanism, Laser beam combination
DOI: 10.3938/jkps.75.45

I. INTRODUCTION

Due to the nonlinear effect and the thermal effect, a single optical fiber has limitations in output power, and ensuring the beam quality at high power is difficult [1]. The beam combination of laser arrays based on adaptive optics can both improve the output power and ensure higher beam quality. At the same time, the application of a fiber array optical system in laser transmission can overcome the shortcomings of the traditional, single, large-aperture telescope optical system, such as heavy weight, large size and high price [2].

The phase and the tip-tilt errors of the beam need to be controlled in the beam combination, especially the tip-tilt phase errors have a great influence on the combining effect [2]; as a result, a device that can control the tip-tilt of beam more rapidly and efficient should be studied. The traditional structure of a tip-tilt control is a fast steer mirror [3], which has a low mechanical resonance frequency and is not easy to realize when the control bandwidth is high [4]. The adaptive fiber optics collimator (AFOC) is an effective way to compensate tilting aberration. It can directly drive the end of an optical fiber with a high mechanical resonance frequency and a compact structure, which is beneficial to array integration and module expansion.

In recent years, a growing number of institutions have studied AFOCs. In 2005, Beresnev and Vorontsov from the University of Dayton designed and developed

*E-mail: littlesnow@126.com; wangliang.ciomp@foxmail.com

Fig. 1. (Color online) Traditional AFOC structure.

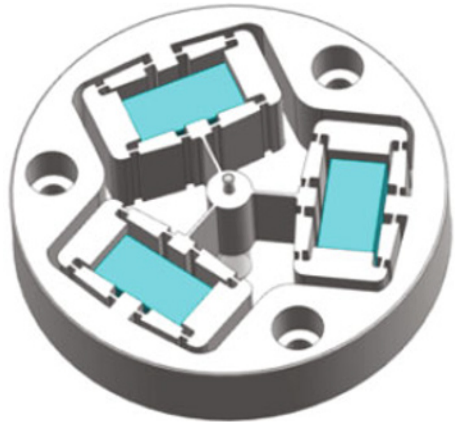

Fig. 2. (Color online) Novel fiber positioner structure.

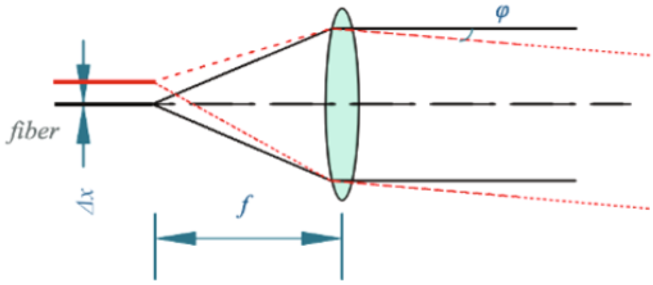

Fig. 3. (Color online) Optical scheme of laser beam emission.

an AFOC for free-space optical communication for the first time and carried out coherent combination (phase-locked) and incoherent combination experiments on optical fiber array system beams, as well as laser beam projection experiments on random rough-surface extended targets [5–7]. In 2011, Geng Chao from the Institute of Optics and Electronics, Chinese Academy of Sciences designed a similar AFOC structure for laser beam combination and laser beam coupling [4,8]. In 2014, Zhi Dong from the National University of Defense Technology designed AFOC based on flexible hinges for high-energy laser beam combination [9,10].

The traditional AFOC structure is shown in Fig. 1, the cross flexible rod is driven by four piezoelectric bimorph actuators, which can only provide a very limited driving force, usually less than 1 N. The optical fiber positioner designed in this research is a novel AFOC based on the flexible hinge amplification mechanism and has high precision and a large driving force, so it can achieve large displacement outputs and fast tip-tilt control. We believe that it has a good prospects for use in future laser-beam combination applications.

II. WORKING PRINCIPLE

1. Structure design of fiber positioner

The adaptive fiber collimating array consists of two parts: the fiber positioner and the collimating lens.

The fiber positioner was developed, as shown in Fig. 2. Three identical flexible hinge amplification mechanisms are distributed equality on a circle, each flexible hinge mechanism is driven by a piezoelectric stack actuator to realize an output displacement of one direction, and the synthesis of the motions of three directions control the fiber tip-tilt movement together to combine the laser beam arrays. This structure has the advantages of being both a piezoelectric ceramic with small size, high resolution, fast response, and large driving force (usually hundreds of N) and a flexible hinge with small stiffness coefficient, no mechanical friction, and high sensitivity.

The end of the optical fiber is located in the focal plane of the collimating lens. The optical scheme of laser beam emission is shown in Fig. 3.

If the deviation of the end of the optical fiber along the x-axis is Δx and the focal length of the collimating lens is f, then the deflection angle of the outgoing beam relative to the optical axis is φ. Due to the small deflection angle, it can be approximately expressed as

$$\varphi \approx \tan\varphi \approx \frac{\Delta x}{f}. \tag{1}$$

If the focal length f of the collimating lens is determined, the dynamic range of tip-tilt control (namely, the deflection angle φ) is proportional to the displacement Δx; thus, increasing the displacement and the speed of the deflection can effectively improve the dynamic range of tilt control, which is related to the structural parameters of the optical fiber positioner. We will further study the

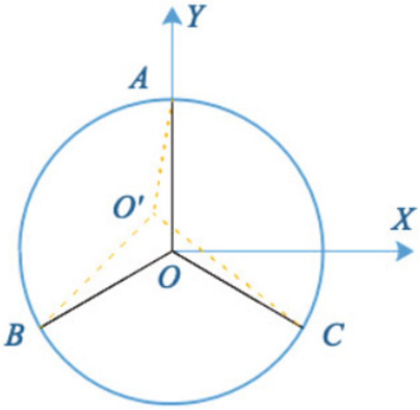

Fig. 4. (Color online) Motion principle of the fiber positioner from O to O' while A, B, and C presents the intersections of the output ends of the amplifying mechanism and the central ring.

structure design and the optimization of flexible hinges amplification mechanism.

2. Resultant displacement

The three amplification mechanisms work together to drive the fiber in both the X direction and the Y direction. The principle of the motion for a simplified section of the end of the optical fiber is shown in Fig. 4.

The initial length is l, when moving from point O to point O', the length of each flexible bars varies :

$$\begin{aligned} \Delta l_A &= \sqrt{x^2+(y-l)^2}-l\ , \\ \Delta l_B &= \sqrt{\left(x+\frac{\sqrt{3}}{2}l\right)^2+\left(y+\frac{1}{2}l\right)^2}-l\ , \\ \Delta l_C &= \sqrt{\left(x-\frac{\sqrt{3}}{2}l\right)^2+\left(y+\frac{1}{2}l\right)^2}-l\ , \end{aligned} \tag{2}$$

If the elongation direction of the output displacement of each bar is assumed to be positive and the shortening direction to be negative, the maximum achievable displacements of the fiber positioner in the X direction and the Y direction are, respectively,

$$\begin{aligned} \Delta x &= \frac{\sqrt{3}}{2}\Delta l_B-\frac{\sqrt{3}}{2}\Delta l_C\ , \\ \Delta y &= -\Delta l_A+\frac{1}{2}\Delta l_B+\frac{1}{2}\Delta l_C\ . \end{aligned} \tag{3}$$

The three amplification mechanisms have the same structure, and the maximum output displacement of each mechanism is equal to $\pm\Delta$, so the maximum possible output along the X-axis is $\pm\sqrt{3}/2\Delta$, and the maximum possible output along the Y-axis is $\pm 2\Delta$. Compared with the structure in which the naked fiber is driven directly along the X-axis and the Y-axis, a larger output displacement can be achieved.

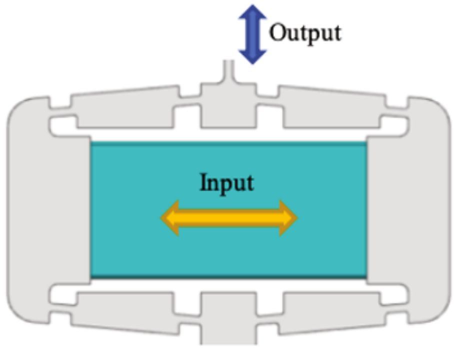

Fig. 5. (Color online) Flexible hinge amplifying mechanism.

III. STRUCTURE ANALYSIS OF THE AMPLIFYING MECHANISM

As shown in Fig. 5, bidirectional piezoelectric ceramics were mounted in the flexible hinge mechanism basement, which is equivalent to an amplifying mechanism, and amplifies the displacement of the piezoelectric ceramics. The bi-polar piezoelectric ceramics were selected as actuators and can move bidirectionally to push and pull the optical fiber.

The flexible structure and the piezoelectric ceramic were connected to form a frictionless movement amplification mechanism. The flexible hinges were commonly made of a rectangular blank removing two symmetric cut-outs with profiles of different forms, such as circular, oval, triangular, and corner-filleted. Different hinges have different characteristics [11,12], and the hinge structure used in this paper is corner-filleted hinge.

The horizontal direction is the input movement direction of the piezoelectric ceramic, and the vertical direction is the output movement direction of the amplification mechanism. When a voltage is applied to the piezoelectric ceramic to make it elongate, the mechanism on the left and the right sides of the actuator is affected by a force F, and an input displacement along the x-axis is generated. The displacement on both sides of the actuator is δx, the total input displacement is $2\delta x$, and the output displacement obtained through the amplification mechanism along the y-axis is $2\delta y$, thus, the amplification ratio is

$$R=\frac{2\delta y}{2\delta x}=\frac{\delta y}{\delta x}\ . \tag{4}$$

Due to the low stiffness of the left and the right connecting bars, the mechanism is prone to deformation, which will affect the amplification ratio of the mechanism, so achieving the ideal amplification ratio will be

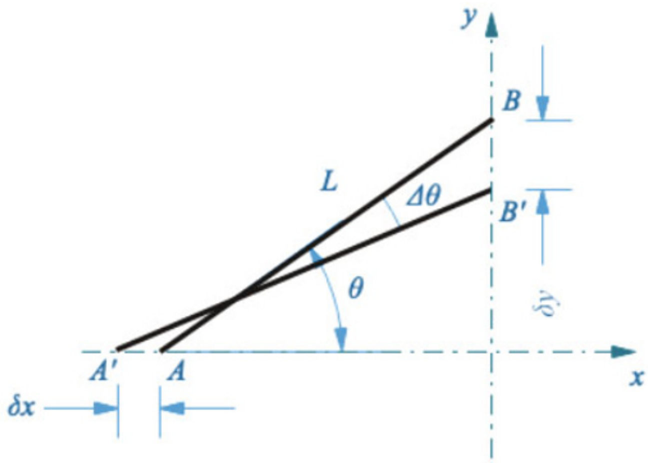

Fig. 6. (Color online) Schematic diagram of the amplifying mechanism.

difficult in practical applications. When the piezoelectric actuator is not strictly perpendicular to the left and the right connecting bars during installation, the force on the mechanism is uneven, this can be corrected by designing a boss structure on the left and the right sides of the actuator; the stiffnesses of the bars can be increased, and the effect of the deformation of the bar on the amplification ratio can be reduced.

1. Geometric relation

As the flexible hinge amplifying mechanism is a symmetrical mechanism, a quarter of it was taken for analysis. Fig. 6 shows the geometry of the quarter amplifying mechanism. According to Ref. 13, Pokines and Garcia derived the amplification ratio in terms of trigonometric functions as

$$R_0 = \frac{\delta y}{\delta x} = \left| \frac{\sin(\theta) - \sin(\theta - \Delta\theta)}{\cos(\theta) - \cos(\theta - \Delta\theta)} \right| . \quad (5)$$

The amplification ratio of a flexible hinge amplification mechanism derived from the triangle relationship is only related to the angle θ and its variation. According to the derivation of the geometric relation, the output displacement is

$$\delta y = L\cdot\sin(\theta) - L\cdot\sin\left(\arccos\left(\frac{\delta x + L\cdot\cos(\theta)}{L}\right)\right) , \quad (6)$$

and the amplification ratio of the mechanism can be obtained as follows:

$$R_1 = \frac{\delta y}{\delta x} = \frac{L\cdot\sin(\theta) - L\cdot\sin\left(\arccos\left(\frac{\delta x + L\cdot\cos(\theta)}{L}\right)\right)}{\delta x} . \quad (7)$$

The amplification ratio from Eq. (7) involves many variables $(L, \theta, \delta x)$ and the formula is complicated without

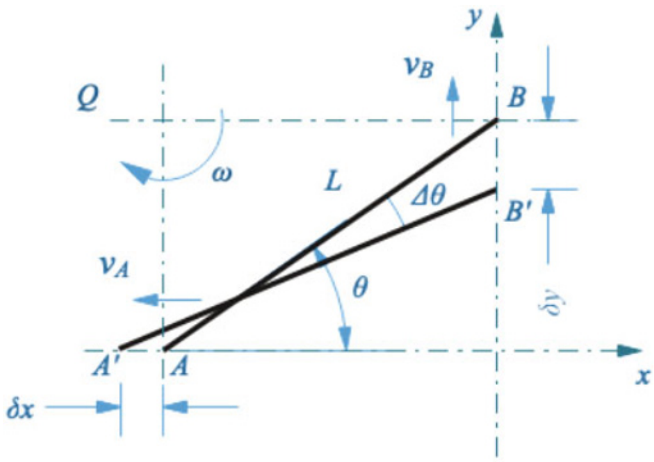

Fig. 7. (Color online) Kinematic analysis of the amplifying mechanism.

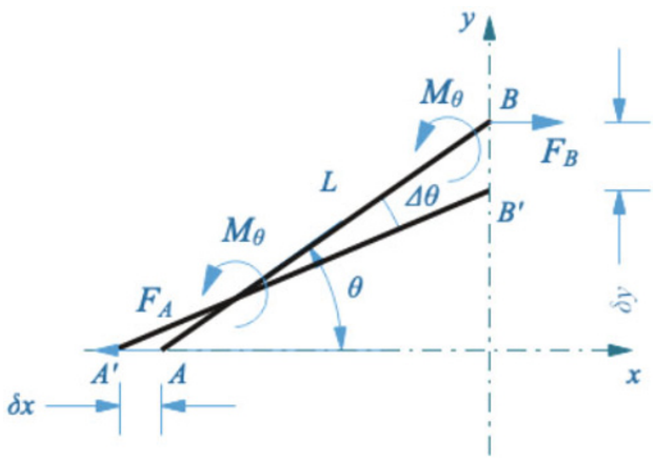

Fig. 8. (Color online) Force analysis of the amplifying mechanism.

considering the kinematics principle and elastic beam theory; thus the displacement amplification ratio obtained from the geometric relationship is not very accurate.

2. Kinematic analysis

Figure 7 shows the quarter kinematic model of the flexible hinge amplifying mechanism. Assuming that the equivalent arm rotates around Q, and ω is the angular velocity of rotation. The velocities of A and B are, respectively,

$$\begin{cases} \nu_A = \dfrac{\delta x}{\delta t} = \omega \cdot OA \\ \nu_B = \dfrac{\delta y}{\delta t} = \omega \cdot OB. \end{cases} \quad (8)$$

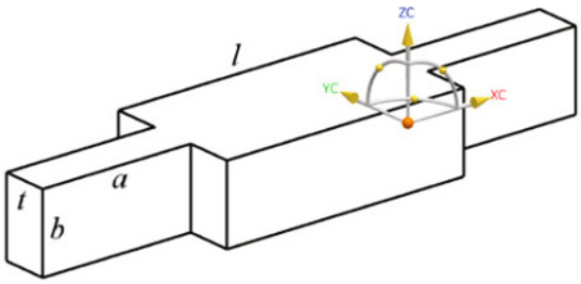

Fig. 9. (Color online) Flexible hinge coordinate system.

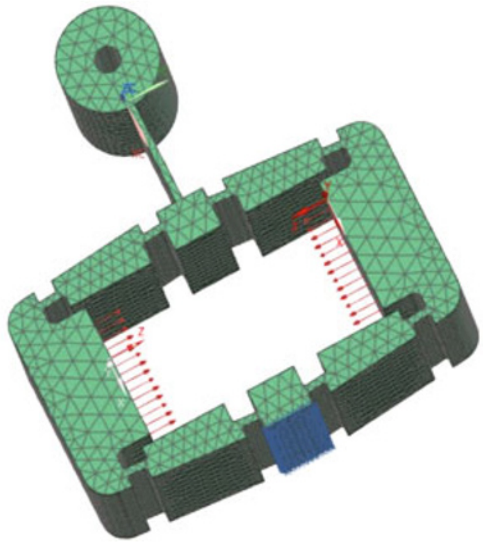

Fig. 10. (Color online) FEM analysis model of the fiber positioner.

Thus, the amplification ratio is

$$R_2 = \frac{\nu_B}{\nu_A} = \frac{OB}{OA} = \cot\theta. \tag{9}$$

The amplification ratio of the mechanism according to the kinematic theory can be seen to be only related to the angle θ and to decreases with increasing θ.

3. Elastic beam theory analysis

Figure 8, under the assumption that $F_A = F_B = F$, shows the quarter force analysis of the flexible hinge amplifying mechanism. The moment on arm AB is

$$2M_\theta = FL\sin\theta = 2K_\theta\Delta\theta; \tag{10}$$

the force along the arm AB is

$$F_L = F\cos\theta = K_L\Delta L. \tag{11}$$

Thus, at point A,

$$F\delta x = F_L\Delta L + 2M_\theta\Delta\theta, \tag{12}$$

and the amplification ratio is

$$R_3 = \frac{L\cos\theta}{\frac{2K_\theta\cdot\cos^2\theta}{K_L\cdot L\sin\theta} + L\sin\theta}. \tag{13}$$

According to elastic beam theory, the flexible hinge can be simplified as a uniform beam, so the flexible hinge coordinate system is established as shown in Fig. 9.

The static characteristics of a flexible hinge can be expressed by using a compliance matrix C, and its inverse matrix is the stiffness matrix $K = C^{-1}$ [14,15], the compliance equation is

$$X = CF, \tag{14}$$

where

$$\begin{aligned} X &= [\delta x, \delta y, \delta z, \theta x, \theta y, \theta z]^T, \\ F &= [F_x, F_y, F_z, M_x, M_y, M_z]^T. \end{aligned} \tag{15}$$

The compliance matrix of the flexible hinge amplifying mechanism is composed of structural parameters (a is the length of the flexible bar, t is its thickness, b is its width) and material parameters (E is the elastic modulus, G is the shear modulus) and can be expressed as

$$C = \begin{bmatrix} \frac{a}{Ebt} & 0 & 0 & 0 & 0 & 0 \\ 0 & \frac{4a^3}{3Ebt^3} + \frac{a}{Gbt} & 0 & 0 & 0 & \frac{6a^2}{Ebt^3} \\ 0 & 0 & \frac{4a^3}{3Eb^3t} + \frac{a}{Gbt} & 0 & \frac{-6a^2}{Eb^3t} & 0 \\ 0 & 0 & 0 & \frac{a}{Gkbt^3} & 0 & 0 \\ 0 & 0 & \frac{-6a^2}{Eb^3t} & 0 & \frac{12a}{Eb^3t} & 0 \\ 0 & \frac{6a^2}{Ebt^3} & 0 & 0 & 0 & \frac{12a}{Ebt^3} \end{bmatrix}. \tag{16}$$

As for the mechanism considered in this research, only the planar stiffness need to be considered, so

$$\begin{cases} K_L \approx \dfrac{Ebt}{a}, \\ K_\theta \approx \dfrac{Ebt^3}{12a}, \end{cases} \tag{17}$$

and the amplification ratio from Eq. (13) can be written as

$$R_3 = \frac{L\cos\theta}{\dfrac{t^2\cdot\cos^2\theta}{6\cdot L\sin\theta} + L\sin\theta}. \tag{18}$$

The amplification ratio of the mechanism, according to elastic beam theory, can be seen to be related to t, L, and θ.

IV. MODAL ANALYSIS

The finite-element (FEM) analysis model is established as shown in Fig. 10, based on the structure of

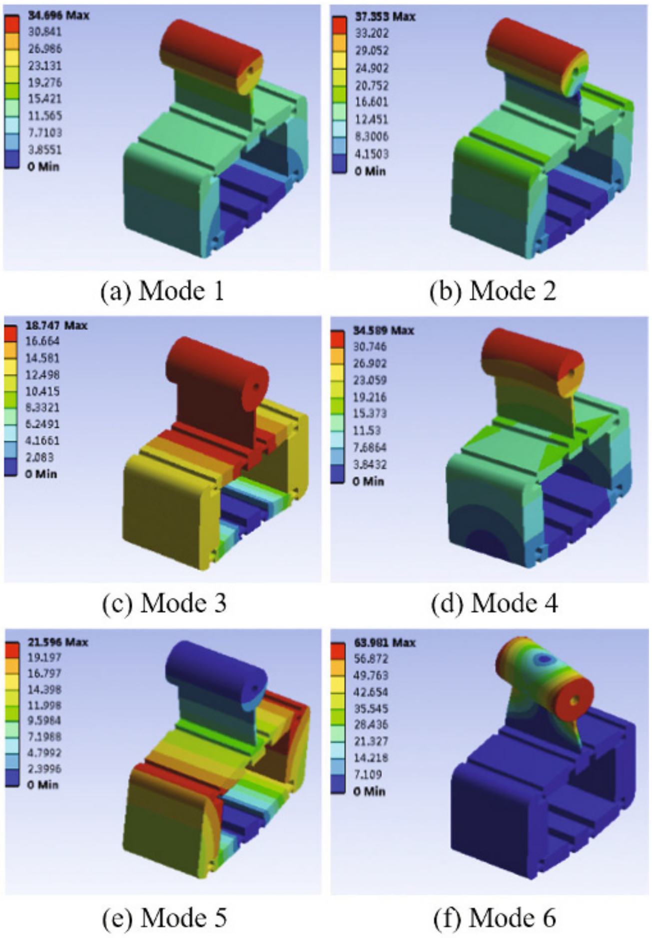

Fig. 11. (Color online) First six orders of the mode shape of the vibration.

Fig. 5, by using a modal analysis of the fiber positioner's amplification mechanism. The first 6 orders mode shape of fiber positioner amplification mechanism were obtained and are shown in Fig. 11, and the resonant frequencies were calculated.

The mode shape of Mode 1 and Mode 2 are deflection centered along the y-axis in the x, y plane, the mode shape of Mode 3 is deformation along the output displacement direction y-axis, which has great influence in application, and the mode shape of Mode 4 is deflection centered along the y-axis in the y, z plane. The analysis showed that the first-order resonant frequency is about 758 Hz, and the third-order resonant frequency is about 2049 Hz. Different mode orders have various deformations; thus, the resonant frequencies obtained by using the modal analysis are need to be avoided in applications.

V. PERFORMANCE EXPERIMENT

According to the designed structure of fiber positioner based on the flexible hinge amplification mechanism, the object of the positioner was made as shown in Fig. 12, where Fig. 12(a) is without installation of the actuators, and Fig. 12(b) is with installation of the actuators. The main purpose of the performance experiment was to verify the driving ability of the flexible hinge amplification mechanisms in the positioner to the end of the optical fiber, namely, the realizable dynamic range of displacement and the frequency response characteristics.

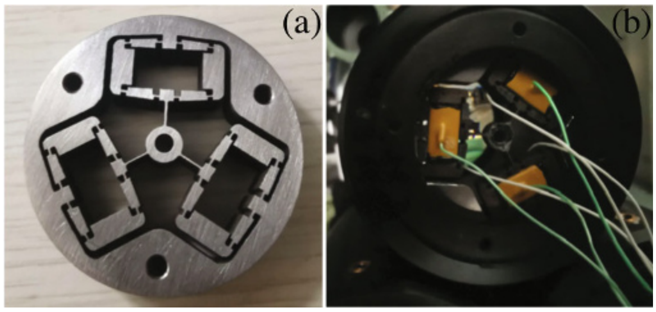

Fig. 12. (Color online) The fiber positioner.

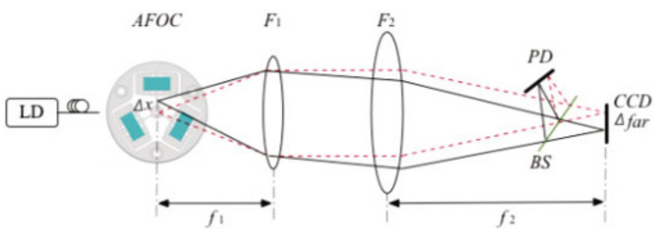

Fig. 13. (Color online) Performance experiment scheme for the fiber positioner.

The layout of the performance experiment on the fiber positioner is shown in Fig. 13. The fiber is located on the focal plane of the collimating lens F1. The collimating beam is focused in the far field by using the large lens F2. A camera is used to observe the far-field spot, and a photodiode (PD) is used to detect the light intensity. If the displacement of the fiber in the focal plane of collimating lens is Δx, the displacement of the far-field spot is Δfar, the focal length of the collimating lens F_1 is f_1, the focal length of the large lens F_2 is f_2, then $\Delta far = f_2/f_1 \times \Delta x$.

1. Displacement range

The coordinate system is shown in Fig. 9, and the positioner response curve between the input voltage and the output displacement is shown in Fig. 14. When the driving voltage changes from 0 V to 150 V, the displacement change response curves for the positioner in the X-axis and that in the Y-axis are shown in Fig. 14, where Fig. 14(a) is for the positive X-axis direction, Fig. 14(b) is for the negative X-axis direction, Fig. 14(c) is for the positive Y-axis direction, and Fig. 14(d) is for the negative Y-axis direction. Because of the need to overcome

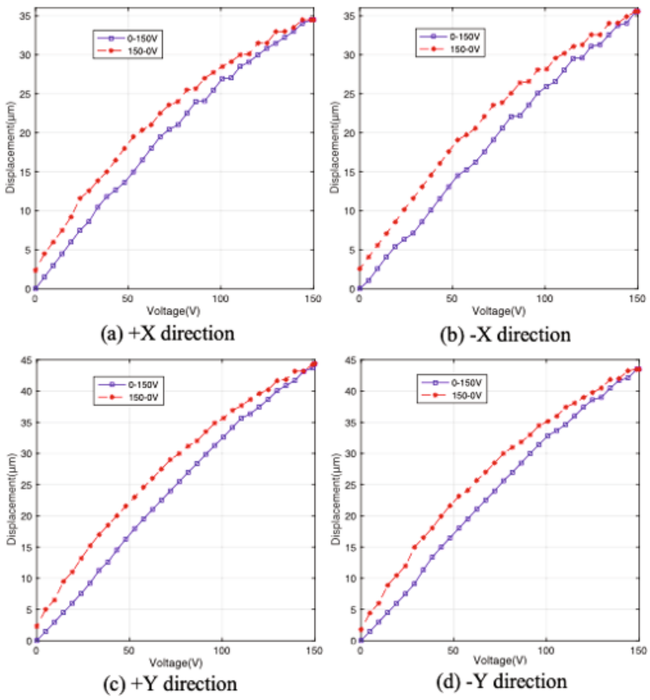

Fig. 14. (Color online) Response curves for the output displacement *vs.* input voltage.

the weight of the end of the fiber, the direction with a large amount of adjustment is taken as the vertical direction to compensate for the effect of gravity on the displacement.

As can be seen from Fig. 14, due to the hysteresis effect of the piezoelectric actuator, the response curve obtained when the voltage is increased from 0 V to 150 V does not coincide with the response curve when the voltage is decreased from 150 V to 0 V, which is similar to the response curve of the actuator. The output displacement is basically linear in the applied voltage. The results show that the structure of the fiber positioner designed in this research can achieve a displacement change in the horizontal X direction of about ± 35 μm and a displacement change in the vertical direction of about ± 44 μm. In other words, a deflection angle from -0.35 mrad to $+0.35$ mrad can be achieved in the horizontal direction while a deflection angle from -0.44 mrad to $+0.44$ mrad can be achieved in the vertical direction, with a large dynamic range.

2. Frequency response characteristics

The frequency response of the fiber positioner was tested. The signal generator outputs sinusoidal signals of 1 Hz $\sim$ 1 kHz, and the drive signal of the piezoelectric actuator is obtained after amplification by the high voltage amplifier. The frequency response curve for the fiber positioner is shown in Fig. 15.

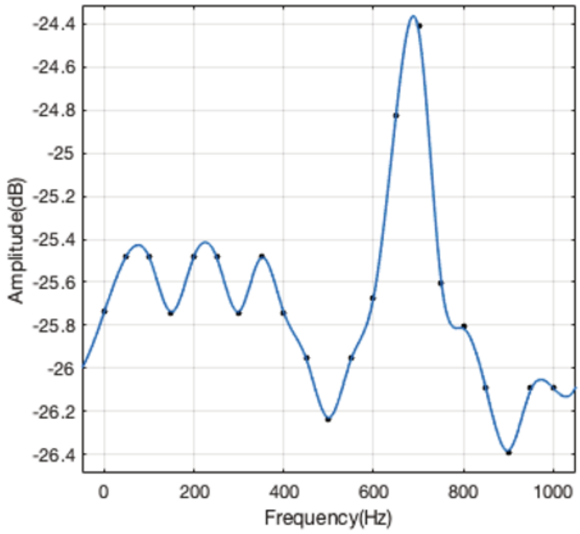

Fig. 15. (Color online) Frequency response curve for the fiber positioner.

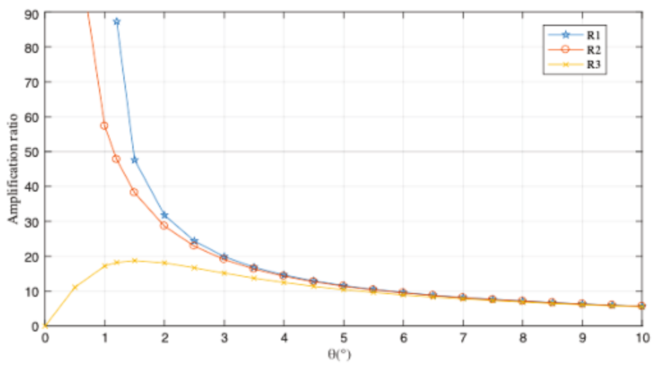

Fig. 16. (Color online) Amplification ratio *vs.* angle.

Figure is shown that the first-order resonant frequency is about 700 Hz, and the effective bandwidth is about 400 Hz. This is consistent with the results of the finite-element simulation, which proves the correctness of the simulation analysis.

VI. DISCUSSION

The amplification ratio *vs.* angle is shown in Fig. 16. When the angle θ is small (less than 2°), the amplification ratios R1 and R2 are large, and as θ increases, R1 and R2 both decreases while R3 first increases to a maximum and then decreases. When the angle θ is more than 5°, the amplification ratios R1, R2 and R3 are nearly constant and as θ increases, the amplification ratios slowly decrease.

The amplification ratio *vs.* the thickness of the flexible bar is shown in Fig. 17. Only R3 is related to the thickness of the flexible bar t. As can be seen in Fig. 16, as t

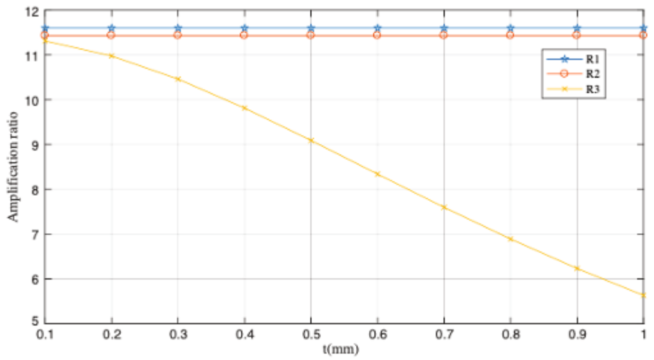

Fig. 17. (Color online) Amplification ratio *vs*. thickness of the flexible bar.

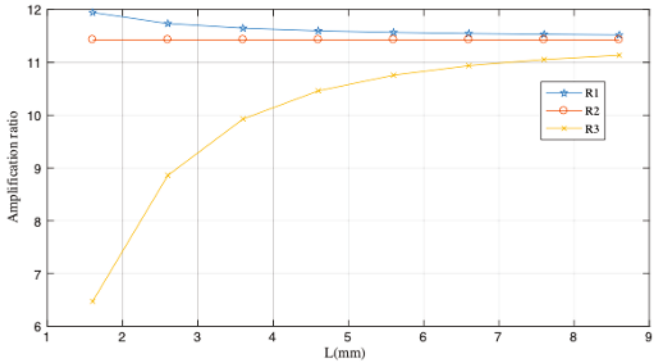

Fig. 18. (Color online) Amplification ratio *vs*. equivalent length of the arm.

increases, the amplification ratio R3 decreases. However, if t is small, the difficulty of processing will be increased.

The amplification ratio *vs*. equivalent length of the arm is shown in Fig. 18. As the length L increases, the change in R1 is not obvious while R3 increases first rapidly and then slowly. However, if the length is large, the structure size will increase.

Taking all factors into consideration, the final equivalent length, angle and thickness are, respectively, chosen as 5.5 mm, 6°, and 0.3 mm. Accordingly, we compared the theoretical analysis, simulation calculation and experimental results for the machined fiber positioner, as shown in Table 1.

The simulation calculation is analyzed based on the model in Fig. 10. We applied a fixed constraint to the blue part of the model and an input displacement to the area of the model red arrows. We performed a static analysis on the model, and obtained the output displacement, so we were able to calculate the amplification ratio of the output displacement to input displacement.

The amplification ratio R1 was derived from geometric relationships, and R2 was derived from the kinematic analysis. Both R1 and R2 were obtained under the ideal condition of not considering the friction force. We can use either R1 or R2 to estimate ideal amplification ratio limit; for example, we can choose R2 for simplicity and

Table 1. Amplification ratio obtained by using different methods.

Analytical Method	R1	R2	R3	FEM	Experiment
Amplification Ratio	8.66	8.14	7.89	7.27	4.89

convenience or choose R1 for considering more factors, thus, the friction force is the main cause of the difference between the theoretical models and the simulation. R3 is derived from elastic beam theory by considering the force of the flexible hinge, and the obtained amplification ratio is close to the actual and the simulated amplification ratio, so calculating and estimating the actual amplification ratio by R3 is a better approach.

The render shows that in both the theoretical and the simulation analyses, the calculations were carried out using a single amplifying mechanism while in the experiment, the whole test was carried out using a fiber positioner composed of three amplifying mechanisms. During the test, one amplifying mechanism works while the other two amplifying mechanisms do not work. Table 1 shown that the amplification measured in the experiment is relatively small, which is mainly because the stiffness and friction force of the mechanical structure may lead to a reduction in the output displacement of the actuator when the actuators were installed while the one amplification mechanism needs to bear the reaction force of the other two amplification mechanisms. The next optimization should reduce the mechanical friction or choose materials with small modulus of elasticity to improve the amplification ratio of the amplification mechanisms in the fiber positioner.

VII. CONCLUSION

This paper puts forward a novel fiber positioner structure based on the flexible hinge amplification mechanism, The working principle was introduced, the theoretical model was established, and the influence of different parameters on the amplification ratio was analyzed based on various theories. The analysis results showed that the novel fiber positioner can achieve a larger amplification, and the experimental results showed that deflection angles from -0.35 mrad to $+0.35$ mrad coule be achieved in the horizontal direction while deflection angles from -0.44 mrad to $+0.44$ mrad could be achieved in the vertical direction. The first-order resonant frequency was found to be about 700 Hz. The structure is to be further optimized according to the analysis results, and showed good prospects for applications.

ACKNOWLEDGMENTS

The authors would like to thank Mr. Liu for helpful discussions and gratefully acknowledge support by The Excellent Young Scientists Fund of the Science and Technology Development Foundation of Jilin Province, China (20180520076JH).

REFERENCES

[1] D. Sabourdy *et al.*, Electron. Lett. **38**, 692 (2002).
[2] M. A. Vorontsov *et al.*, IEEE J. Sel. Top. Quantum Electron. **15**, 269 (2009).
[3] H. K. Wang *et al.*, Opt. Prec. Engin. **21**, 336 (2013).
[4] C. Geng, X. J. Zhang, X. Y. Li and C. H. Rao, Infrared Laser Engin. **40**, 1682 (2011).
[5] L. A. Beresnev *et al.*, Proc. SPIE **7090**, 709001 (2008).
[6] L. A. Beresnev and M. A. Vorontsov, U.S. Patent 8,503,837 (2013).
[7] L. A. Beresnev and M. A. Vorontsov, Proc. SPIE **5895**, 589501 (2005).
[8] C. Geng, X. Y. Li, X. J. Zhang and C. H. Rao, Opt. Commun. **284**, 5531 (2011).
[9] D. Zhi *et al.*, Appl. Optics **53**, 5434 (2014).
[10] D. Zhi *et al.*, Opt. Lett. **41**, 2217 (2016).
[11] J. F. Hu, G. Y. Xu and Machi, Design Manufacture **2**, 127 (2014).
[12] Y. L. Tian, B. J. Shirinzadeh, D. C. Zhang and Y. M. Zhong, Precis. Eng.-J. Int. Soc. Precis. Eng. Nanotechnol. **34**, 92 (2010).
[13] B. J. Pokines and E. Garcia, Smart Mater. Struct. **7**, 105 (1998).
[14] J. H. Kim, S. H. Kim and Y. K. Kwak, Rev. Sci. Instrum. **74**, 2918 (2003).
[15] Y. Koseki, T. Tanikawa, N. Koyachi and T. Arai, Adv. Robot. **16**, 251 (2002).